ADVANCES IN ATMOSPHERIC SCIENCES, VOL. 33, JUNE 2016, 730–742

Impact of Spectral Nudging on the Downscaling of Tropical Cyclones in Regional Climate Simulations

Suk-Jin CHOI[†] and Dong-Kyou LEE[*]

Atmospheric Sciences Program, School of Earth and Environmental Sciences, Korea-USA Weather and Climate Research Center Seoul National University, Seoul 151-747, *Korea*

(Received 5 July 2015; revised 16 December 2015; accepted 8 January 2016)

ABSTRACT

This study investigated the simulations of three months of seasonal tropical cyclone (TC) activity over the western North Pacific using the Advanced Research WRF Model. In the control experiment (CTL), the TC frequency was considerably overestimated. Additionally, the tracks of some TCs tended to have larger radii of curvature and were shifted eastward. The large-scale environments of westerly monsoon flows and subtropical Pacific highs were unreasonably simulated. The overestimated frequency of TC formation was attributed to a strengthened westerly wind field in the southern quadrants of the TC center. In comparison with the experiment with the spectral nudging method, the strengthened wind speed was mainly modulated by large-scale flow that was greater than approximately 1000 km in the model domain. The spurious formation and undesirable tracks of TCs in the CTL were considerably improved by reproducing realistic large-scale atmospheric monsoon circulation with substantial adjustment between large-scale flow in the model domain and large-scale boundary forcing modified by the spectral nudging method. The realistic monsoon circulation took a vital role in simulating realistic TCs. It revealed that, in the downscaling from large-scale fields for regional climate simulations, scale interaction between model-generated regional features and forced large-scale fields should be considered, and spectral nudging is a desirable method in the downscaling method.

Key words: tropical cyclone, spectral nudging technique, dynamic downscaling, regional climate simulation

Citation: Choi, S.-J., and D.-K. Lee, 2016: Impact of spectral nudging on the downscaling of tropical cyclones in regional climate simulations. *Adv. Atmos. Sci.*, **33**(6), 730–742, doi: 10.1007/s00376-016-5061-y.

1. Introduction

The western North Pacific (WNP) is home to the most vigorous tropical cyclone (TC) activity. Severe TCs are of considerable interest for many Asian countries because of the serious impact of their high winds, associated storm surges, excessive rain, and flooding. The coarse resolution of GCMs limits them to simulating TC-like vortices that are broader and weaker than actual TCs. This is often inadequate for simulating meaningful TC activity. The simulated vortices in GCMs usually tend to be lacking in terms of storm track length, a distinct eye, and rain bands, compared with observation, although the frequency of simulated TCs is generally similar to that observed (Wu and Lau, 1992; Haarsma et al., 1993; Tsutsui and Kasahara, 1996; Camargo and Sobel, 2004). In order to address the question of TC activity more directly, RCMs, with their relatively higher spatial resolution, have attracted attention (Camargo et al., 2007; Knutson et al., 2007; Feser and von Storch, 2008). As a dynamical downscaling strategy, RCMs can reproduce regional weather details that are influenced by topography, land–sea contrast, and small-scale atmospheric features. They are forced by large-scale information from global coupled model simulations, and provide regional details embedded within low-resolution lateral boundary data, as well as allow the reproduction of their large-scale variability.

In regional climate simulations, strong internal variability can be generated. In East Asia and the WNP, regional features such as complicated topography, various land surface conditions, warm local ocean conditions, strong seasonal monsoon circulation, and thermal convection, affect internal variability in regional climate simulations. These regional features can lead to systematic errors in long-term integrations of regional climate simulations. For example, Qian et al. (2003) found that the systematic errors of precipitation in their long-term simulation were associated with the steep topography and uncertainties in the moisture processes. Cha and Lee (2009) showed that errors in precipitation were induced by the enhanced surface latent heat flux caused by the warm SST anomaly. The spectral nudging technique can re-

[†] Now at Korea Institute of Atmospheric Prediction Systems, 4F., 35 Boramae-ro 5-gil, Dongjak-gu, Seoul 156-849, Korea

[*] Corresponding author: Dong-Kyou LEE
Email: dklee@snu.ac.kr

duce these problems, maintaining the added values generated by the limited-area model, as discussed by von Storch et al. (2000), Miguez-Macho et al. (2004), Castro et al. (2005), and Cha et al. (2011). The results of regional models using the spectral nudging technique do not deviate from large-scale forcing but sustain the numerical balance, while significant modifications in small-scale features are allowed in regional models.

Although this framework clearly depends on the various sources of large-scale information that are forcing the RCM, it is necessary to determine how successfully RCMs can be used for extended simulations of TCs when using the observed atmospheric state and SSTs as perfect boundary conditions. Modeling studies have been conducted previously for individual TCs as case studies for using the nudging technique, which focused on its positive effects. For example, Wang et al. (2013) examined the effect of the spectral nudging technique in improving a TC simulation over seven days. Yesubabu et al. (2014) conducted three-day simulations for several TC cases using grid nudging. Although the simulations of such studies are successful in terms of mesoscale features, such as track, intensity, or structure of the TC, the effect of the spectral nudging technique on extended-range simulations has not been examined. In cases of long-term simulation studies, a number of studies have reported that the RCM produces bias in terms of TC frequency. For example, Walsh et al. (2004) simulated the regional climate of TCs over eastern Australia for a 30-year period without inserting artificial vortices or relaxing the large-scale component of the observed atmospheric state. Despite the lack of generally accepted threshold detection criteria, they concluded that the model generated too many TCs, as compared to observation. Knutson et al. (2007) also simulated the Atlantic hurricane activity during the TC seasons of a 26-year period. The model resulted in a systematic error of generating a higher TC frequency than observed. Tulich et al. (2011) also showed significant bias in TC frequency in their six-year simulation using the tropical channel of the Advanced Research WRF Model (WRF-ARW), which has only meridional boundaries.

In this context of meaningful predictions of TC activity in an RCM, the objectives of the present study were to examine the ability of the limited-area WRF-ARW model to simulate the three-month TC frequency and track over the WNP for the three-month period of 18 June to 18 September 2002. We analyzed the effect of spectral nudging on the regional climate simulation for TC activity, as well as atmospheric circulation and precipitation over the WNP, and investigated the reasons why an overestimated TC frequency and relative systematic errors were generated in the simulation without spectral nudging.

The organization of the paper is as follows. The next section describes the RCM, experiment setup and observational data used in this study. Section 3 presents the simulation results over the WNP, and section 4 summarizes and concludes the findings.

2. Model description, experiments and data

Version 3.0.1.1 of WRF-ARW (Skamarock et al., 2005) was used in this study, employing the Kain–Fritsch cumulus parameterization scheme for subgrid-scale convection (Kain and Fritsch, 1990, 1993), WSM3 (Hong et al., 2004) for moist processes of grid-scale cloud and precipitation, the Yonsei University scheme (Hong et al., 2006) for the PBL, similarity theory (Monin and Obukhov, 1954) for the surface layer, the NOAH land-surface model (Chen and Dudhia, 2001) for land surfaces, and the RRTM longwave (Mlawer et al., 1997) together with the Dudhia shortwave (Dudhia, 1989) schemes for atmospheric radiation processes. The WRF model was run for a domain of 30-km horizontal grid meshes with 200×240 grid points, covering most of the WNP, and 36 vertical layers with the model top at 50 hPa (Fig. 1).

For this study, the spectral nudging method developed by Miguez-Macho et al. (2004) was used. The equation for spectral nudging is

$$\frac{d\alpha}{dt} = X(\alpha) + G_\alpha w(\eta) \sum_{|n|\leqslant N} \sum_{|m|\leqslant M} K_{mn}(\alpha_{o,mn} - \alpha_{mn}) e^{ik_m x} e^{ik_n y} ,$$

where α is any of the prognostic variables being nudged, X is the model operator, G_α is the nudging coefficient as inverse time, and α_o is the reanalysis variable. Here, α_{mn} and $\alpha_{o,mn}$ are the spectral coefficients of α and α_o, respectively. K_{mn} is the scale-selective nudging coefficient of zero or one. For this study, this was set to 1 when the $m \leqslant 7$ (zonal) and $n \leqslant 6$ (meridional) wave numbers corresponded to wavelengths larger than 1000 km, which is the synoptic scale. k_m and k_n are the wave vector components in the x and y directions, respectively. Note that in this study the characteristic time of the relaxation corresponded to around 3 h, which corresponded to a half cycle of the driving analysis data, available every 6 h. This meant that $G_\alpha = 0.0001\ \mathrm{s}^{-1}$. Because the characteristic time is a kind of free parameter, Miguez-Macho et al. (2004, 2005) set it at 5000 s, approximately 1.39 h. Since using a short relaxation time (large weight coefficient) could suppress the model-generating small-scale details, we chose to use a relatively small value. Alexandru et al. (2009) showed that the model internal variability decreases with an increased coefficient. Also, we used $w(\eta) = (1-\eta)^2$ for a vertical weight function of relaxations, where η is the vertical coordinate from 1 (surface) to 0 (top). In this study, the spectral nudging was applied to the horizontal wind component only.

Model experiments were performed for the three-month period of 18 June to 18 September 2002, during the WNP active typhoon season, to investigate the seasonal march of simulated typhoons with and without the application of spectral nudging. The TC season in 2002 was chosen as the target period because the annual TC frequency over the WNP that year was 26, which is very close to the 30-year climatological frequency of 26.09. The experiment without spectral nudging is referred to here as the CTL run, and the experiment with

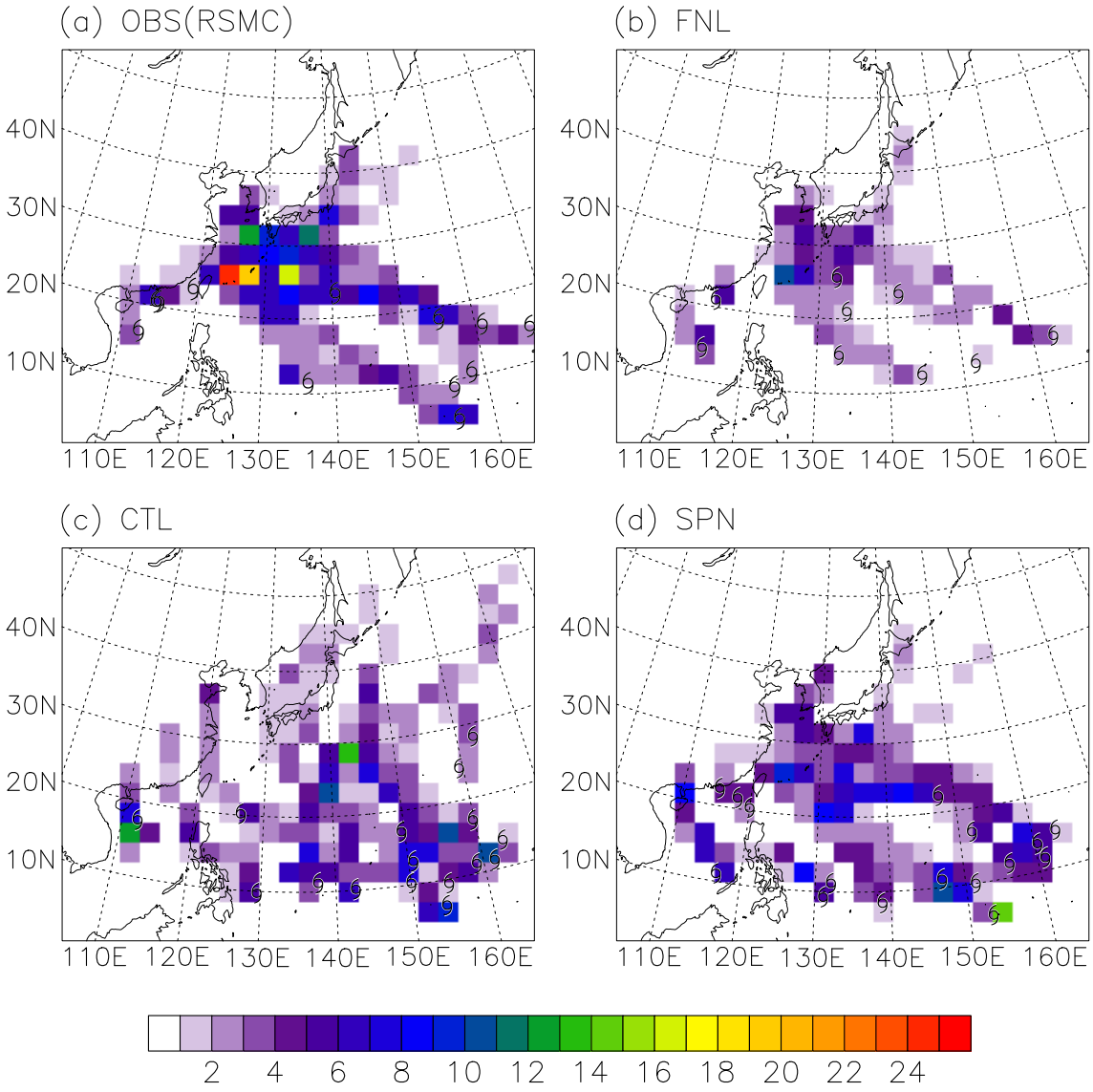

Fig. 1. Track density of TCs in (a) OBS, (b) FNL analysis, (c) CTL and (d) SPN, in the simulation period of 2002. First positions of TCs are marked.

spectral nudging is termed the SPN run. During the simulation period, the observed TC frequency was 14 in the area of interest; however, two TCs were not included within the model domain because they did not influence the East Asian continent. The remaining 12 typhoons are discussed in this paper.

The initial and boundary conditions for the model simulations were obtained from the NCEP Final (FNL) Operational Global analysis data; the data were divided into $1^\circ \times 1^\circ$ grids on 26 standard pressure levels from 1000 to 10 hPa (http://rda.ucar.edu/datasets/ds083.2/). In order to evaluate the simulated wind and geopotential height, ERA-Interim data (Dee et al., 2011) were used. In addition, the 3-h $0.25^\circ \times 0.25^\circ$ merged TRMM and other satellite estimation data of the version 6 3B42 product were used to evaluate the simulated precipitation. The observational data were the best-track data created by the Regional Specialized Meteorological Center (RSMC) Tokyo-Typhoon Center; the data were used to compare the center positions, maximum wind speeds and minimum pressure of the simulated typhoons. Tropical depressions were included in the best-track dataset; however, only TCs with tropical storm intensity or higher are presented in this study.

To define TCs in the simulated results, we used the objective algorithms suggested by Nguyen and Walsh (2001) and Oouchi et al. (2006). In order to evaluate the model performance for the system corresponding to the observed intensity of TCs, some modifications were made. The algorithm defines a simulated TC in an RCM as follows: (1) there must be a local minimum of SLP; (2) the vorticity must be at least 3.5×10^{-5} s^{-1} at 850 hPa; (3) a point must be warm-core, i.e., the total tropospheric temperature anomaly calculated by summing temperature anomalies at 700, 500 and 300 hPa

around the center of the storm must be greater than zero; (4) the mean wind speed in a 500 km^2 region around the center of a point at 850 hPa must be higher than that at 300 hPa; (5) the total tropospheric temperature anomaly has to be greater than 1.5 K; (6) the duration of a model TC satisfying the above conditions must last at least one day; and (7) the surface wind speed has to exceed 17.5 m s^{-1}, which corresponds to tropical storm intensity or higher in the RSMC scale. A simulated TC was identified if all the above criteria were satisfied. After a storm was identified, its track was traced from the identified point.

3. Results

3.1. *Simulated TCs*

Figure 1 shows the first position of all TCs appearing in the RSMC best-track data (OBS), FNL analysis, CTL and SPN at the time when each TC reached the strength of a tropical storm. During the simulation period, 12 TCs were observed within the model domain (Fig. 1a). In the FNL analysis data, which were used for the model boundary conditions, 9 TCs were found using the objective search algorithms of this study (Fig. 1b). Although a lower number of TCs was represented in the FNL data, the first position was in good agreement with OBS. However, the two experiments showed a large difference in the number of simulated TCs. CTL simulated 25 TCs, and SPN simulated 16 TCs (Figs. 1b and c). The spuriously simulated TCs in CTL were concentrated in the area of (10°–20°N, 125°–155°E), east of the Philippines. The formation of a few spurious TCs also occurred in SPN.

To examine the tracks of the TCs in the models and observations, the probability density of TC tracks is also shown in Fig. 1. CTL simulated a relatively high probability density of tracks over the basin of (10°–20°N, 110°–160°E), with an east–west extended pattern. TC tracks in CTL tended not only to have longer curvatures but were also shifted eastward, showing approximate south–north paths. However, SPN showed a high probability density of tracks with a southeast–northwest direction of the two main streams as shown in OBS. The maximum location of the track density over the East China Sea in SPN was comparable to that observed. Furthermore, in SPN the area related to landfall over the Korean Peninsula agreed well with observations.

The characteristics of the simulated TC intensity were examined in terms of the number of TCs versus the minimum central pressure (Fig. 2). The observational distribution of the minimum central pressure was classified by two groups in which a peak of weaker (stronger) TCs appears in the range of 990–980 hPa (940–930 hPa). Both experiments overestimated the mid-intensity TCs. On average, the minimum central pressure in OBS was 956.7 hPa, while those in CTL and SPN were 960.9 and 970.1 hPa, respectively. The CTL central pressure was close to that observed, but that of SPN was about 14 hPa less than observed. Although CTL seemed to show good ability in simulating TCs with intense minimum central pressure, it was found that CTL produced especially higher numbers of weaker TCs, which could be mitigated in SPN. It was notable that the stronger TCs were not sufficiently simulated in SPN. Since the spectral nudging technique provides additional forcing for the model solution to have realistic large-scale flows, the nudged large-scale forcing may dilute small-scale forcing, which is necessary for a TC's strength in its mature stage. On the other hand, the spurious TCs due to erroneous mutual interaction between large-scale flows and small-scale flows could be controlled in SPN.

3.2. *Precipitation and atmospheric circulation*

Figure 3 shows the observed and simulated three-month mean precipitation and wind fields over the entire model domain, excluding the buffer zone. Observationally, the distribution of the precipitation was characterized by two rain

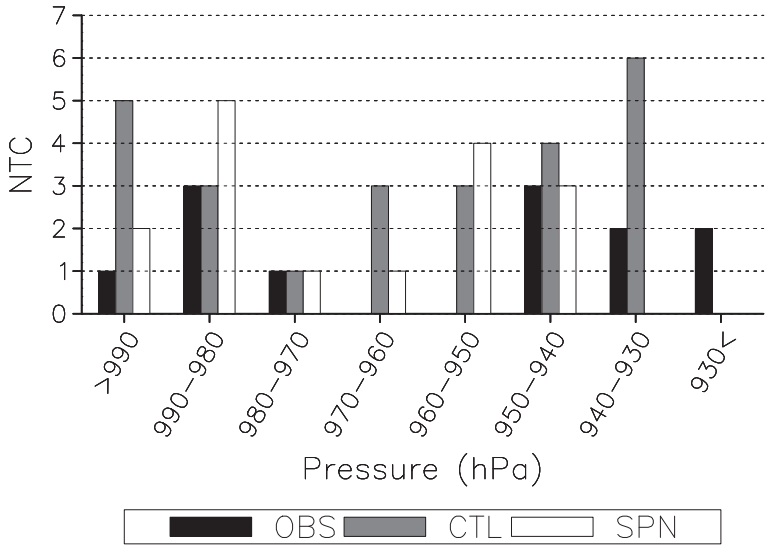

Fig. 2. Number of TCs (NTC) versus minimum central pressure (hPa) in OBS, CTL and SPN.

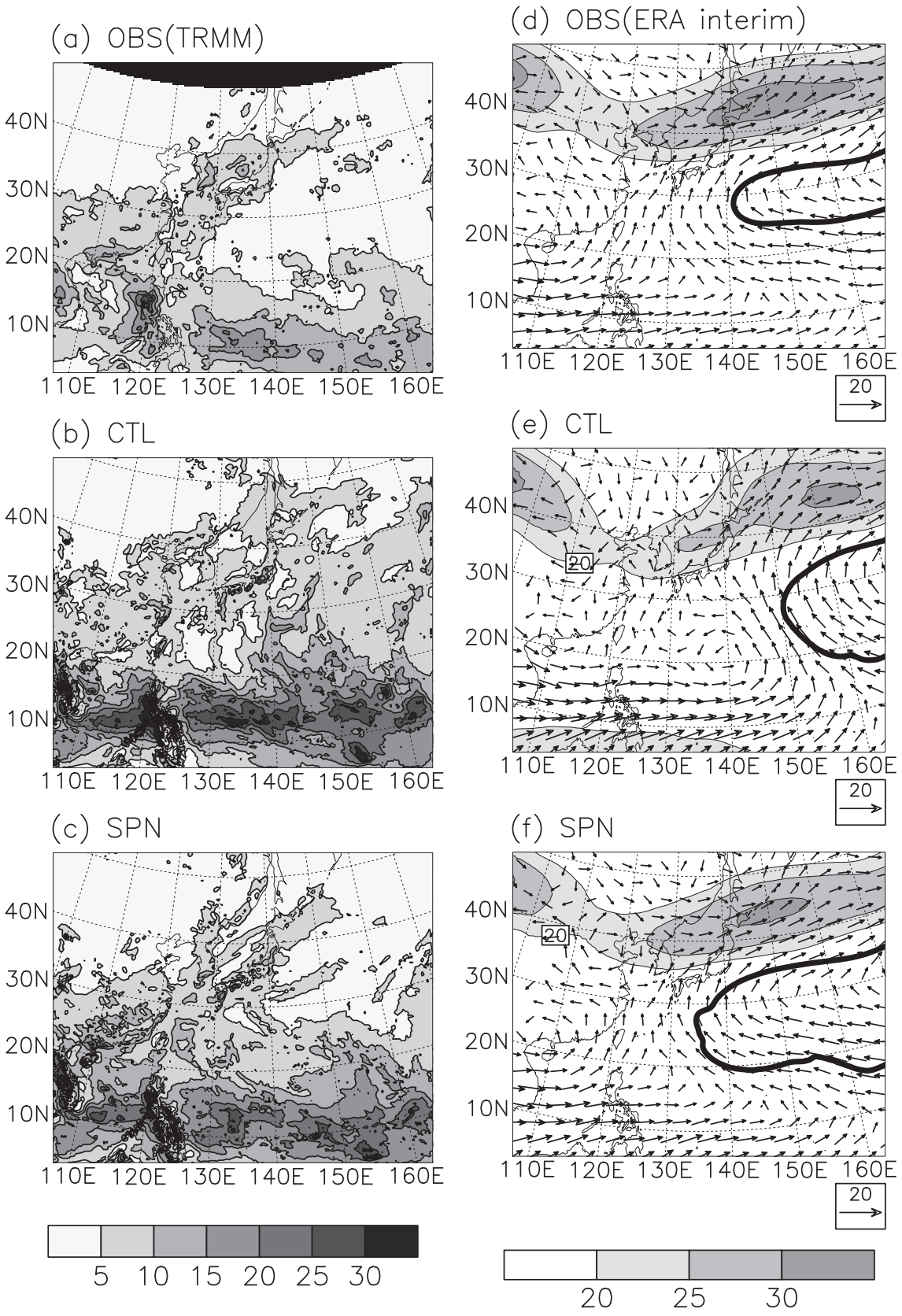

Fig. 3. The three-month mean (a–c) precipitation (mm d^{-1}) and (d–f) 850 hPa wind vector, 200 hPa wind speed (m s^{-1}; contours and shading) and 5880 geopotential height contour (thick solid line), in the (a, d) observation, (b, e) CTL run and (c, f) SPN run. The observed precipitation and atmospheric variables are from TRMM and ERA-Interim data, respectively.

bands and a dry region over the ocean. One of the rain bands extended from the South China Sea to Korea and Japan, which was related to the East Asian summer monsoon (EASM). The other was over the WNP along 10°N, which resulted from the WNP summer monsoon (WNPSM). A relatively dry region appeared in the subtropical high over the WNP, south of Japan, between 20°N and 40°N.

In CTL, the precipitation area related to the EASM was extended eastward over the subtropical WNP, with overestimated precipitation over the dry region southeast of Japan. In addition, the WNPSM precipitation area was overestimated considerably and shifted northward. The overestimated precipitation in CTL was attributed to inaccurate simulations of atmospheric monsoon circulation, as well as TCs. CTL simulated stronger monsoon westerly flows in the area along 10°N, from the west of the Philippines, compared to those observed. The strong westerly flow prevented the WNP subtropical high (WNPSH) from extending westward to East Asia. The simulated 5880 geopotential height contour was displaced to the east by approximately 15°. Consequently, the confluence of westerly and easterly flows over the southern vicinity of the WNPSH turned northward and shifted more eastward than observed. This resulted in intensified cyclonic circulation near 20°N, south of Japan. The overestimated precipitation over the dry area to the southeast of Japan was likely simulated by the migration of convective cells due to the intensified cyclonic circulation, and also by the paths of TCs along the incorrect cyclonic flows (refer to Fig. 1). These results indicate that the mean low-level flow, upper-level flow, and subtropical WNP were not correctly simulated in CTL, which was an unfavorable environment for the development of TCs over the WNP.

In SPN, the overestimated precipitation of the EASM and WNPSM in CTL was considerably reduced. SPN improved the low-level monsoon circulation, and therefore westerly flows along the western boundary of the subtropical high were much weakened, and the anticyclonic circulation of the WNPSH was much intensified. Thus, the eastward extension of the EASM precipitation was significantly corrected. The overestimated WNPSM precipitation was also reduced. It is notable that the precipitation over southern China in SPN was increased and that the precipitation over central and northern China was decreased as compared to CTL. This indicates the importance of interactions between model scale and large-scale variables when an RCM is forced by large-scale fields. The improvement of the simulation of precipitation is evidenced by the spatial correlation coefficients between the simulations and observation. The spatial correlation coefficient over ocean (land) increased from 0.61 (0.61) to 0.78 (0.90) when the spectral nudging technique was applied.

Figure 4 shows the eigenvector of the EOF and the time series of the corresponding first-mode eigenvalue of a six-hourly 925-hPa wind vector during the simulated period. In the observation (ERA-Interim), the first eigenvector accounted for 14.0% of total variance, which was characterized

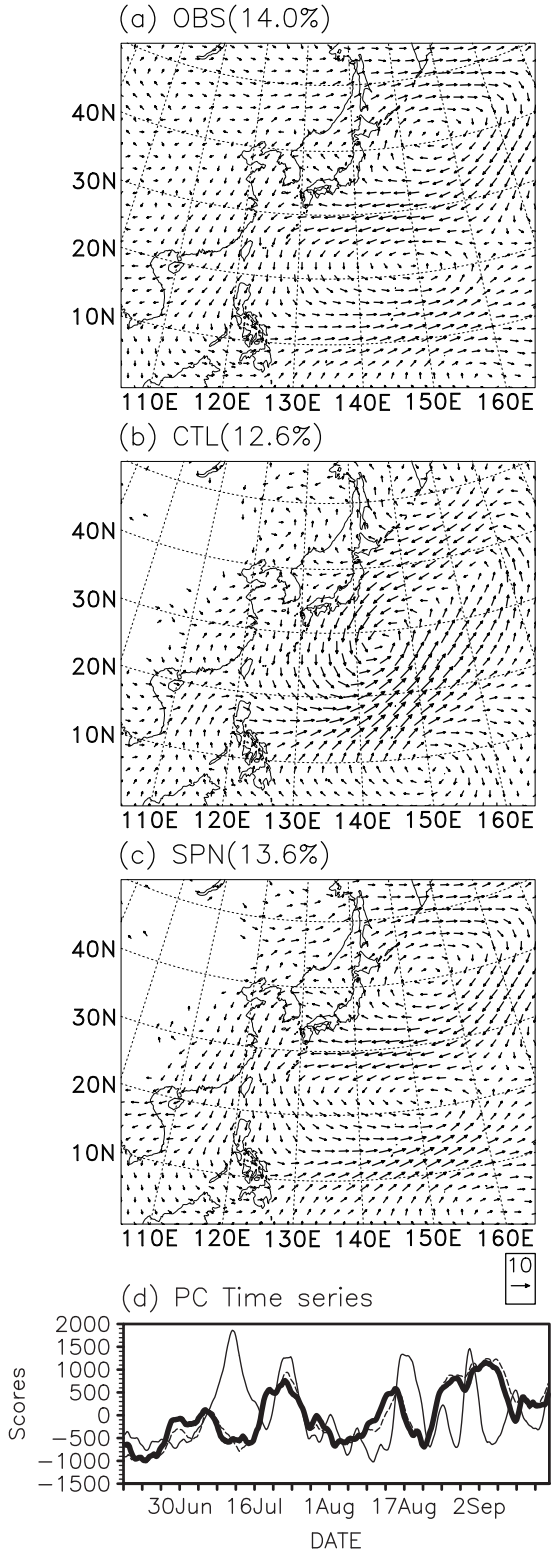

Fig. 4. First-mode eigenvectors and its percentage of total variance, which is shown in the parenthesis, from the EOF analysis of the six-hourly 925-hPa wind vector (units: m s^{-1}) during the total simulated period in (a) OBS (ERA-Interim), (b) CTL and (c) SPN. (d) Corresponding PC time series in OBS (thick solid line), CTL (thin solid line) and SPN (dotted line).

by a dipole pattern of anticyclonic circulation between 30°N and 45°N, and cyclonic circulation along 20°N between 120°E and 160°E (Fig. 4a). The active cyclonic circulation indicated an active monsoon trough, which was also coupled with the anticyclonic circulation. This reflects the intensification of the monsoon trough. The southern branch of the cyclonic circulation extended eastward from the Philippine Sea, thereby covering the southwestern North Pacific. This pattern was also noticeable in the study of Harr and Elsberry (1995). However, in CTL, these patterns were not reproduced, as they were somewhat distorted in the simulation (Fig. 4b). That is, in CTL, the simulated cyclonic circulation dominated over the ocean in the model domain, and the observed anticyclonic circulation east of Japan was not simulated. Thus, an exaggerated strong cyclonic flow was simulated in the southwestern North Pacific in CTL. The observed circulation pattern was reasonably reproduced in SPN but the cyclonic circulation was intensified, with its center having moved eastward (Fig. 4c). It should be noted that in SPN the eigenvector pattern and the corresponding principal component (PC) time series of the 925-hPa wind were closely comparable with observations (Fig. 4d). The PC time series of the observation and SPN indicated intra-seasonal variability with an approximate 20-day cycle, implying that SPN was able to simulate the temporal variability of the atmospheric circulation.

The good agreement of SPN was indicated well by the temporal variation of the cross-correlation coefficient of 500 hPa geopotential height between the simulations and ERA-Interim data (Fig. 5). The simulated atmospheric flows in CTL without the adjustment of the large-scale pattern were readily deviated from the lateral boundary conditions because of a lack of interaction between the large-scale field and TCs within the model. It was noticeable that the mature stage of TCs being under 945 hPa was likely to decrease the cross-correlation coefficient in CTL. Although CTL allowed the model-generating small-scale details more than SPN, the stronger TCs in CTL tended to reduce the reliability of the simulations, with inaccurate large-scale wind fields.

Figure 6 shows the 3-month mean spectral variances of the kinetic energy over the entire domain at the height of 10 m, and the corresponding ratio of CTL to SPN. There was little difference between the two simulations at the small scale, under the wavelength of 1000 km (wave number of 7), which corresponds to the cutoff wave number of the spectral nudging technique used in this study. However, the difference at the large scale was greater because of the distorted atmospheric flows. Although the variance of kinetic energy was small at the small scale, the ratio of the spectra of CTL to those of SPN showed a large value at the small scale, compared with that at the large scale (Fig. 6b). It can be seen that the ratio had a peak at the wave number of 17 (wavelength of 450 km), which can correspond to an average TC radius. CTL resolved more kinetic energy at this wave number than SPN, as more TCs were simulated. Thus, it was concluded that small-scale circulations in CTL were readily affected by the large amount of kinetic energy in the large-scale circulations.

3.3. *Large-scale patterns at the formation of TCs*

To investigate the large-scale patterns at the formation of TCs, the classification method of Lee et al. (2008) was used for the experiments in this study. Through the use of the low-level wind flow and surge direction of the satellite-based wind data at the first time of the best-track data (Table 1), Lee et al. (2008) classified the formation of TCs into six synoptic patterns; easterly wave (EW); northeasterly flow (NE); coexistence of northeasterly and southwesterly flow (NE-SW); southwesterly flow (SW); monsoon confluence (MC); and monsoon shear (MS). The set of criteria was established on the magnitude of the zonal and meridional wind components in the four $5^\circ \times 5^\circ$ latitude–longitude quadrants. In this study, the same criteria were used for classifying model-simulated synoptic flow patterns associated with TC formation (Table 1), but the formation time was taken at the first time of an

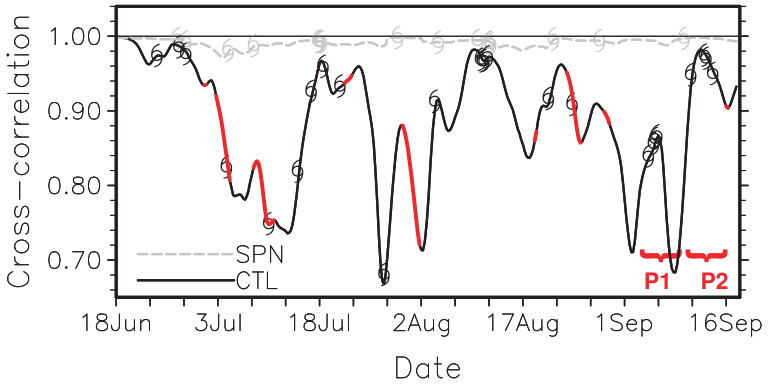

Fig. 5. Temporal variation in the cross-correlation coefficient of geopotential height at 500 hPa between the simulations and ERA-Interim data. The TC marks indicate when TCs appeared for the first time. The duplicated red lines of CTL are marked to indicate the time when TCs under 945 hPa existed. P1 indicates the period of 2–6 September, and P2 is the period of 11–14 September, which are also referred to in Fig. 7.

Table 1. Criteria used for classifying the six synoptic flow patterns associated with the 124 TC formations, which were applied to identify strong (> 5 m s^{-1}) and weak (< 2 m s^{-1}) average zonal (U) and meridional (V) wind components and their directions (+/−) at low levels (850 and 925 hPa) in the four 5° × 5° latitude–longitude quadrants with respect to the system center. Blank indicates null values.

	NE quadrant		NW quadrant		SW quadrant		SE quadrant	
Synoptic pattern	U	V	U	V	U	V	U	V
EW	(−) strong	(−) weak	(−) strong				(−) weak	
NE	(−) strong		(−) strong	(−) strong				
NE-SW				(−) strong	(+) strong			
SW	(−) strong			(−) weak	(+) strong		(+) strong	
MC					(+) strong		(+) strong	
MS	(−) strong				(+) strong			

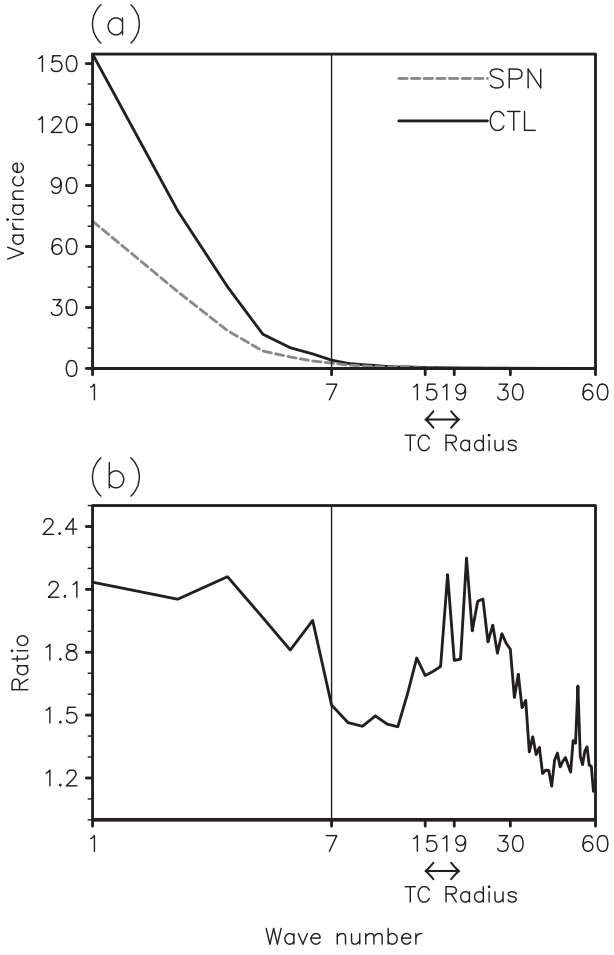

Fig. 6. (a) Spectral variances of the kinetic energy at the height of 10 m in CTL (solid) and SPN (dashed). (b) Ratio of the spectra between CTL and SPN (CTL/SPN). The wave number 7 is the top wave number to nudge. The wave numbers of 15 to 19 correspond to a radius of TC, which is indicated by arrows of the x-axis.

isolated circular of local minimum SLP associated with an identified TC occurrence, which was archived by backward tracing from the first time of the TC track. On average, the time interval between the formation time and the first time of simulated TC tracks was about 48 hours. A more detailed description for the classification method can be found in Lee et al. (2008).

As a result of this classification, five classes of low-level flow patterns were identified for both experiments (all except the EW pattern) (Table 2). However, four cases were only identified in the observation (all except the EW and MC pattern). It is important to note that, regarding the classification in the observation, FNL analysis data were used for the low-level wind flow and surge direction, and the first time and location of the RSMC best-track data were also employed. In CTL (SPN), there were 5(3) NE cases, 4(4) NE-SW cases, 1(2) SW cases, 10(5) MC cases, and 1(2) MS cases. CTL simulated the MC pattern twice more than SPN, and even 4 TCs of non-classified patterns, which were not shown in SPN. Figure 7 shows the composite 925 hPa flows for each pattern. The low-level flow patterns of this study correspond well with those analyzed in Lee et al. (2008). CTL enhanced the southern quadrants with respect to the center of a TC system, as compared to SPN. In CTL, the non-classification patterns indicated TC cases that were generated near the eastern boundary of the model domain, due to the lack of interaction with large-scale flows forced from the lateral boundary. A typical example of a non-classified pattern is shown in Fig. 7f.

Higher numbers of CTL TCs in the MC case were mostly attributed to the enhanced wind speed in the southern quadrant, which resulted in an inaccurately active monsoon trough (refer to Fig. 3e). Harr and Elsberry (1995) pointed out that the enhancement of the monsoon trough was associated with active TCs in lower latitudes of the WNP. It should also be noted that monsoon-related flows are responsible for multiple TC geneses. For example, during the period P1 (2–6 Septem-

Table 2. Distribution of the number of formation cases associated with the synoptic flow patterns.

Synoptic pattern	CTL	SPN	OBS (FNL)
EW	0	0	0
NE	5	3	4
NE-SW	4	4	5
SW	1	2	1
MC	10	5	0
MS	1	2	2
Others	4	0	0

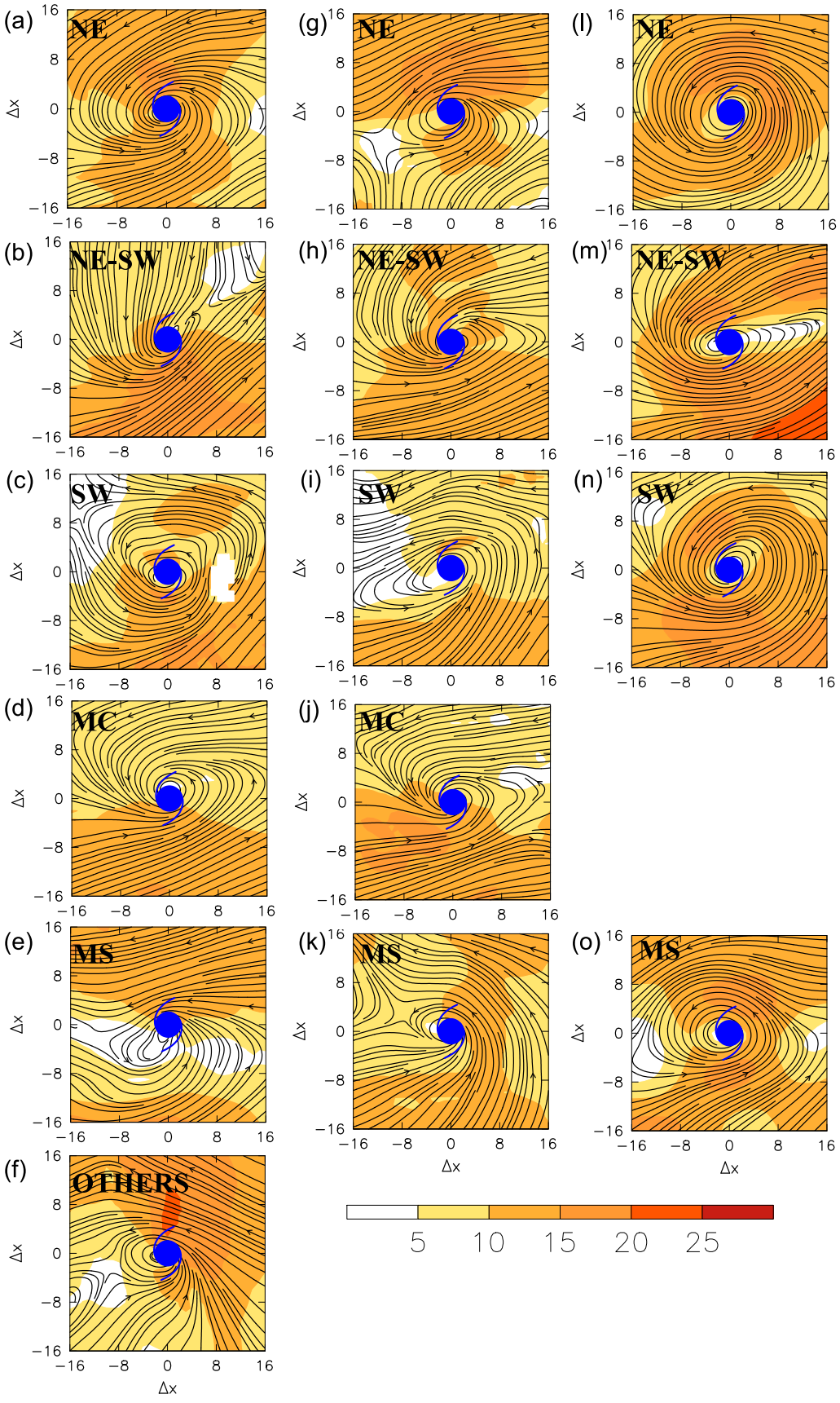

Fig. 7. Composite 925-hPa streamlines and wind speed (m s^{-1}; shaded) for the (a, g, l) NE, (b, h, m) NE-SW, (c, i, n) SW, (d, j) MC and (e, k, o) MS synoptic patterns, in (a–e) CTL, (g–k) SPN and (l–o) OBS. (f) "Others" indicates the non-classified patterns. *x* indicates a grid length in unit of 30-km.

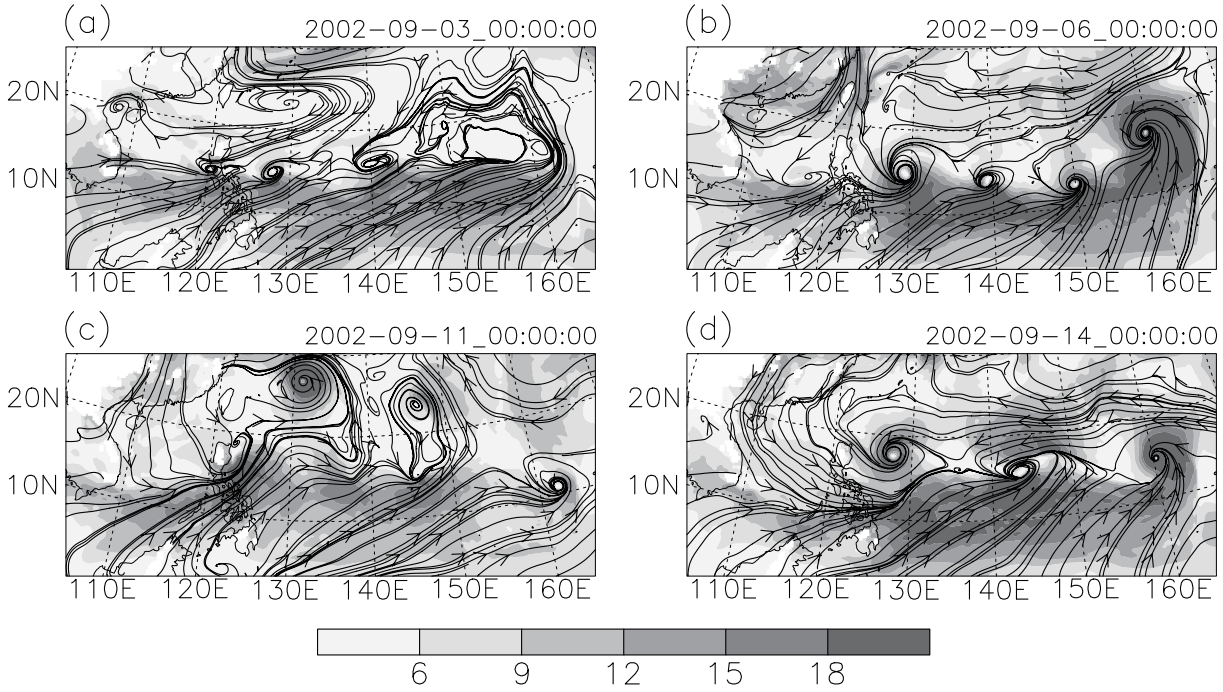

Fig. 8. 925-hPa streamline and wind speed (m s^{-1}; shaded) in the CTL at (a) 0000 UTC 3 September 2002 and (b) 0000 UTC 6 September 2002 for the period P1, and (c) 0000 UTC 11 September 2002 and (d) 0000 UTC 14 September 2002 for the period P2.

ber) and P2 (11–14 September), the 925 hPa streamlines and wind speed successfully diagnosed the synoptic conditions associated with the simultaneous formation (Fig. 8). For the first date of P1, strong westerly flows along 10°N sustained for four days prior to the formation of the TCs in CTL (Fig. 8a). A time series of confluent regions was collocated with the maximum gradient of the zonal flow and the cyclonic shear extending from east of the Philippines to the western boundary of the model domain. The zonal and meridional winds were also gradually intensified over the four days, leading to the simultaneous formation of two NE-SW pattern TCs and two MC TCs (Fig. 8b). About five days later, a similar streamline and wind speed appeared again in the same region in CTL (Figs. 8c and d). For the first date of P2, the monsoonal westerly flow in CTL was strong in the region of the monsoon shear line. In P2, the simultaneous formation of three TCs of the MC pattern occurred, while the wind speed was intensified over three days. In the observation and SPN, however, there was no significant change in flow patterns during the two periods (not shown).

The erroneous wind induced increased surface fluxes of moisture and latent heat though friction-induced convergence, which resulted in increased equivalent potential temperature at the surface. In the surface layer scheme used in this study (Oncley and Dudhia, 1995), the parameterization for the surface moisture flux is based on eddy perturbation quantities, such as the friction velocity (u_*) and characteristic moisture (q_*). The surface moisture flux is then given by u_*q_*. The enhanced friction velocity by the erroneous wind and wind shear in CTL played a role in increasing the surface fluxes of moisture and latent heat. This relationship is known as a wind-induced surface heat exchange (WISHE) in several studies (Emanuel, 1986; Emanuel et al., 1994; Craig and Gray, 1996). Figure 9 shows the temporal variations of the three-hourly frictional velocity, surface moisture flux, surface latent heat flux, and equivalent potential temperature at the surface, averaged over the ocean at (10°–20°N, 125°–165°E), in which most of the simulated TCs were formed. The temporal variations of all variables were significantly correlated with each other. CTL tended to simulate a stronger friction velocity over the entire period, compared with SPN. The stronger friction velocity tended to simulate more surface moisture and more latent heat in CTL than SPN. Due to the moisture and heat enhancement from the sea surface, the equivalent potential temperature at the lowest model level also increased, which could have fueled the initiation and intensification of TCs.

4. Summary and conclusions

In this study, we investigated the simulated formation and development of TCs over the WNP for a 3-month period using the WRF model and boundary data forced by FNL analysis data. The effect of the spectral nudging method on the seasonal frequency and intensity of simulated TCs was analyzed. The simulation without spectral nudging (CTL) showed not only an overestimated frequency and unrealistic tracks of TCs, but unreasonable seasonal mean fields of precipitation and low-level circulation too. In CTL, the summer monsoon precipitation along 10°N over the WNP was con-

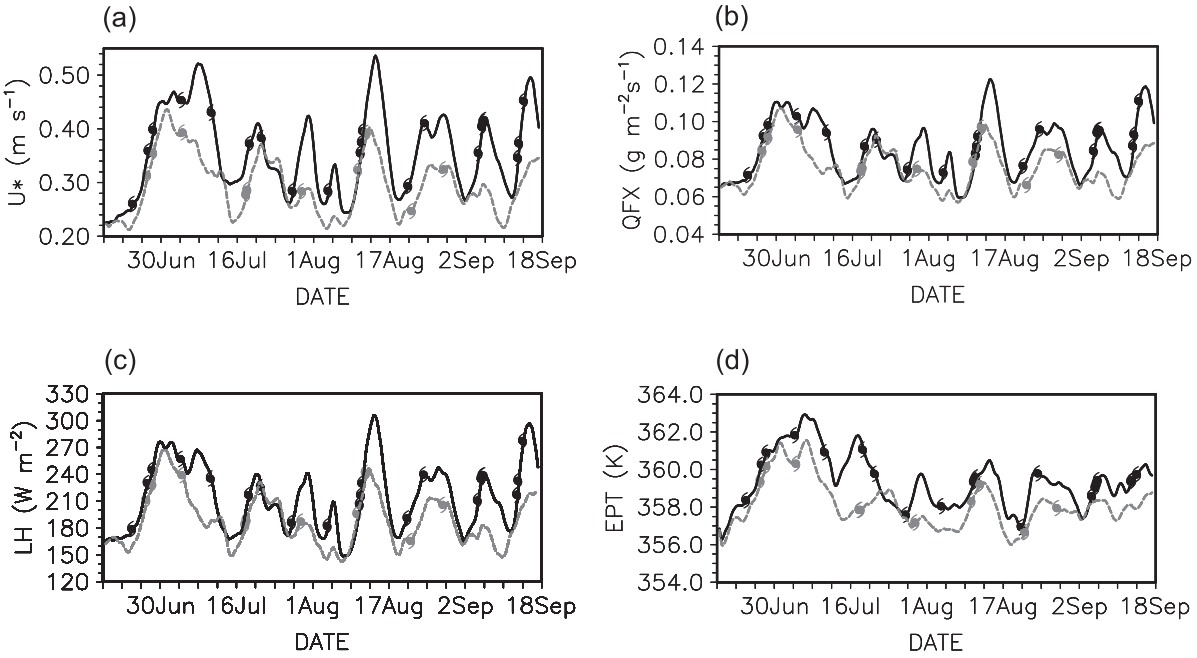

Fig. 9. Time series of (a) frictional velocity, (b) moisture flux, (c) latent heat flux and (d) equivalent potential temperature, at the lowest model level in CTL (thick line) and SPN (dashed line). The TC marks indicate when TCs appeared for the first time.

siderably overestimated and northward-shifted due to inaccurately simulated atmospheric monsoon circulation, as well as TC frequency and tracks. CTL simulated strong westerly flow and a weakened WNPSH. The maximum intensity of TCs also tended to be more excessive. The number of spurious TCs was increased due to a kind of climate drift effect in the later part of the simulation period.

The overestimated number of TCs in CTL was attributed to the multiple TC formation associated with the inaccurate monsoon trough, which was mainly modulated by enhanced large-scale flows greater than 1000 km. The enhanced kinetic energy of the large-scale flow in CTL implied that the model could not correctly reproduce the observed atmospheric circulation due to the lack of interaction between large-scale flows provided by the lateral boundary and model-generated flows. Consequently, the model simulated incorrect or dynamically imbalanced large-scale flows in the long integration of the model. These results are consistent with several studies (e.g., Rinke and Dethloff, 2000; Lee et al., 2004; Miguez-Macho et al., 2004). Rinke and Dethloff (2000) indicated that most errors in climate simulations over the Arctic using a regional model resulted from differences in wavelengths longer than 1000 km, which corresponds to the cutoff of large-scale flows in this study.

In the classification of the low-level wind patterns at the formation of TCs, CTL simulated twice as many TCs of the MC pattern defined by Lee et al. (2008) than those in SPN. More simulated TCs of the MC pattern in CTL was mostly attributed to enhanced westerly monsoon flows in the southern quadrant with respect to the TC center. Furthermore, enhanced wind speed caused the model to produce more moisture content and increased temperature at the lowest level over the ocean, which in turn initiated more typhoons by increasing the conditional instability.

It should be emphasized that a realistic monsoon circulation takes a vital role in simulating realistic TCs. Owing to the realistic low-level monsoon circulation in SPN, the westerly flow along the western boundary of the model domain and the anticyclonic circulation of the WNPSH were much improved. SPN reduced the exaggerated number of TCs and erroneous rainfall of the major rain bands of the EASM and WNPSM, due to the simulated spurious wind field compared to CTL. The interaction between the large-scale environment and internal variability in the regional model was reasonable as a result of using the spectral nudging technique.

The summer monsoon over East Asia and the WNP is affected by many factors, such as the subtropical high in the WNP, the midlatitude low-pressure systems and blocking highs, land surface processes related to soil moisture and snow depth, and the SST (Weng et al., 2004). Cha and Lee (2009) investigated the systematic errors of simulated precipitation associated with the summer monsoon by applying the spectral nudging technique. In this study, the spurious TC formation, which was attributed to inaccurate monsoonal atmospheric flow fields, was corrected by the proper simulation of the synoptic background using the spectral nudging technique.

Regional climate simulations are also dependent on physical parameterization schemes, especially cumulus parameterization and grid-scale resolvable schemes. Used in this study, the Kain–Fritsch scheme, whose convection is determined by CAPE, can overestimate convection and precipita-

tion over the ocean. Strong convection can trigger unreasonable positive feedback during a long period of simulation. In the future, the effect of convection in longer simulations of TCs should be investigated, and it is also necessary to further investigate the intensity of simulated TCs through the coupling of RCMs with ocean models.

Acknowledgements. This work was funded by the Korea Meteorological Administration Research and Development Program under grant KMIPA 2015–2083. We thank the anonymous reviewers for their constructive suggestions.

REFERENCES

Alexandru, A., R. De Elia, R. Laprise, L. Separovic, and S. Biner, 2009: Sensitivity study of regional climate model simulations to large-scale nudging parameters. *Mon. Wea. Rev.*, **137**, 1666–1686.

Camargo, S. J., and A. H. Sobel, 2004: Formation of tropical storms in an atmospheric general circulation model. *Tellus A*, **56**, 56–67.

Camargo, S. J., H. L. Li, and L. Q. Sun, 2007: Feasibility study for downscaling seasonal tropical cyclone activity using the NCEP regional spectral model. *Int. J. Climatol.*, **27**, 311–325.

Castro, C. L., R. A. Pielke Sr., and G. Leoncini, 2005: Dynamical downscaling: Assessment of value retained and added using the regional atmospheric modeling system (RAMS). *J. Geophys. Res.*, **110**, D05108, doi: 10.1029/2004JD004721.

Cha, D.-H., and D.-K. Lee, 2009: Reduction of systematic errors in regional climate simulations of the summer monsoon over East Asia and the western North Pacific by applying the spectral nudging technique. *J. Geophys. Res.*, **114**, D14108, doi: 10.1029/2008JD011176.

Cha, D.-H., C.-S. Jin, D.-K. Lee, and Y.-H. Kuo, 2011: Impact of intermittent spectral nudging on regional climate simulation using Weather Research and Forecasting Model. *J. Geophys. Res.*, **116**, D10103, doi: 10.1029/2010JD015069.

Chen, F., and J. Dudhia, 2001: Coupling and advanced land-surface/hydrology model with the Penn State/NCAR MM5 modeling system. Part I: Model description and implementation. *Mon. Wea. Rev.*, **129**, 569–585.

Craig, G. C., and S. L. Gray, 1996: CISK or WISHE as the mechanism for tropical cyclone intensification. *J. Atmos. Sci.*, **53**, 3528–3540.

Dee, D. P., and Coauthors, 2011: The ERA-Interim reanalysis: Configuration and performance of the data assimilation system. *Quart. J. Roy. Meteor. Soc.*, **137**, 553–597.

Dudhia, J., 1989: Numerical study of convection observed during the winter monsoon experiment using a mesoscale two-dimensional model. *Atmos. Sci.*, **46**, 3077–3107.

Emanuel, K. A., 1986: An air-sea interaction theory for tropical cyclones. Part I: Steady state maintenance. *J. Atmos. Sci.*, **43**, 585–604.

Emanuel, K. A., J. D. Neelin, and C. S. Bretherton, 1994: On large-scale circulations in convecting atmospheres. *Quart. J. Roy. Meteor. Soc.*, **120**, 1111–1144.

Feser, F., and H. von Storch, 2008: A dynamical downscaling case study for typhoons in Southeast Asia using a regional climate model. *Mon. Wea. Rev.*, **136**, 1806–1815.

Haarsma, R. J., J. F. B. Mitchell, and C. A. Senior, 1993: Tropical disturbances in a GCM. *Climate Dyn.*, **8**, 247–257.

Harr, P. A., and R. L. Elsberry, 1995: Large-scale circulation variability over the tropical western North Pacific. Part I: Spatial patterns and tropical cyclone characteristics. *Mon. Wea. Rev.*, **123**, 1225–1246.

Hong, S.-Y., J. Dudhia, and S.-H. Chen, 2004: A revised approach to ice microphysical processer for the bulk parameterization of clouds and precipitation. *Mon. Wea. Rev.*, **132**, 103–120.

Hong, S.-Y., Y. Noh, and J. Dudhia, 2006: A new vertical diffusion package with an explicit treatment of entrainment processes. *Mon. Wea. Rev.*, **134**, 2318–2341.

Kain, J. S., and J. M. Fritsch, 1990: A one-dimensional entraining/detraining plume model and its application in convective parameterization. *J. Atmos. Sci.*, **47**, 2748–2802.

Kain, J. S., and J. M. Fritsch, 1993: Convective parameterization for mesoscale models: The Kain-Fritsch scheme. *The Representation of Cumulus Convection in Numerical Models*, K. A. Emanuel and D. J. Raymond, Eds., Amer. Meteor. Soc., 246 pp.

Knutson, T. R., J. J. Sirutis, S. T. Garner, I. M. Held, and R. E. Tuleya, 2007: Simulation of the recent multidecadal increase of Atlantic hurricane activity using an 18-km-grid regional model. *Bull. Amer. Meteor. Soc.*, **88**, 1549–1565.

Lee, C.-S., K. K. W. Cheung, J. S. N. Hui, and R. L. Elsberry, 2008: Mesoscale features associated with tropical cyclone formations in the western North Pacific. *Mon. Wea. Rev.*, **136**, 2006–2022.

Lee, D. K., D. H. Cha, and H. S. Kang, 2004: Regional climate simulation of the 1998 summer flood over East Asia. *J. Meteor. Soc. Japan*, **82**, 1735–1753.

Miguez-Macho, G., G. L. Stenchicov, and A. Robock, 2004: Spectral nudging to eliminate the effects of domain position and geometry in regional climate model simulations. *J. Geophys. Res.*, **109**, D13104, doi: 10.1029/2003JD004495.

Miguez-Macho, G., G. L. Stenchicov, and A. Robock, 2005: Regional climate simulations over North America: Interaction of local processes with improved large-scale flow. *J. Climate*, **18**, 1227–1246.

Mlawer, E. J., S. J. Taubman, P. D. Brown, M. J. Iacono, and S. A. Clough, 1997: Radiative transfer for inhomogeneous atmosphere: RRTM, a validated correlated-k model for the longwave. *J. Geophys. Res.*, **102**(D14), 16 663–16 682.

Monin, A. S., and A. M. Obukhov, 1954: Basic laws of turbulent mixing in the surface layer of the atmosphere. *Contributions of the Geophysical Institute of the Slovak Academy of Sciences*, **24**(151), 163–187.

Nguyen, K. C., and K. J. E. Walsh, 2001: Interannual, decadal and transient greenhouse simulation of tropical cyclone-like vortices in a regional climate model of the South Pacific. *J. Climate*, **14**, 3043–3054.

Oncley, S. P., and J. Dudhia, 1995: Evaluation of surface fluxes from MM5 using observations. *Mon. Wea. Rev.*, **123**, 3344–3357.

Oouchi, K., J. Yoshimura, H. Yoshimura, R. Mizuta, S. Kusunoki, and A. Noda, 2006: Tropical cyclone climatology in a global-warming climate as simulated in a 20 km-mesh global atmospheric model: Frequency and wind intensity analyses. *J. Meteor. Soc. Japan*, **84**, 259–276.

Qian, J.-H., A. Seth, and S. Zebiak, 2003: Reinitialized versus continuous simulations for regional climate downscaling. *Mon. Wea. Rev.*, **131**, 2857–2874.

Rinke, A. and K. Dethloff, 2000: On the sensitivity of a regional

Arctic climate model to initial and boundary conditions. *Clim. Res*., **14**(2), 101–113.

Skamarock, W. C., J. B. Klemp, J. Dudhia, D. O. Gill, D. M. Barker, W. Wang, and J. G. Powers, 2005: A description of the Advanced Research WRF Version 2. NCAR Tech. Note TN-468+STR.

Tsutsui, J. I., and A. Kasahara, 1996: Simulated tropical cyclones using the national center for atmospheric research community climate model. *J. Geophys. Res*., **101**, 15 013–15 032.

Tulich, S. N., G. N. Kiladis, and A. Suzuki-Parker, 2011: Convectively coupled Kelvin and easterly waves in a regional climate simulation of the tropics. *Climate Dyn*., **36**, 185–203, doi: 10.1007/s00382-009-0697-2.

von Storch, H., H. Langerberg, and F. Feser, 2000: A spectral nudging technique for dynamical downscaling purposes. *Mon. Wea. Rev*., **128**, 3664–3673.

Walsh, K. J. E., K.-C. Nguyen, and J. L. McGregor, 2004: Fine-resolution regional climate model simulations of the impact of climate change on tropical cyclones near Australia. *Climate Dyn*., **22**, 47–56.

Wang, H., Y. Q. Wang, and H. M. Xu, 2013: Improving simulation of a tropical cyclone using dynamical initialization and large-scale spectral nudging: A case study of Typhoon Megi (2010). *Acta Meteorologica Sinica*, **27**(4), 455–475, doi: 10.1007/s13351-013-0418-y.

Weng, H., A. Sumi, Y. N. Takayabu, M. Kimoto, and C. Li, 2004: Interannual-interdecadal variation in large-scale atmospheric circulation and extremely wet and dry summers in China/Japan during 1951-2000 part I: spatial patterns. *J. Meteor. Soc. Japan*, **82**, 775-788.

Wu, G. X., and N. C. Lau, 1992: A GCM simulation of the relationship between tropical storm formation and ENSO. *Mon. Wea. Rev*., **120**, 958–977.

Yesubabu, V., C. V. Srinivas, S. S. V. S. Ramakrishna, and K. B. R. R. Hari Prasad, 2014: Impact of period and timescale of FDDA analysis nudging on the numerical simulation of tropical cyclones in the Bay of Bengal. *Natural Hazards*, **74**, 2109–2128.